RADIATIVE SHOCK OVERSTABILITY OF FINITE SIZE OBJECTS

RUTH DGANI

INFRARED PROCESSING AND ANALYSIS CENTER, JET PROPULSION LABORATORY

CALIFORNIA INSTITUTE OF TECHNOLOGY

POSTAL ADDRESS: IPAC, CALTECH 100-22, PASADENA, CA 91125

INTERNET: KNILL@IPAC.CALTECH.EDU

AND

NOAM SOKER

MATHEMATICS-PHYSICS, ORANIM–UNIVERSITY DIVISION

TIVON 36910, ISRAEL

INTERNET: SOKER@PHYS4.TECHNION.AC.IL

ABSTRACT

We investigate the radiative shock overstability for finite size objects. We follow the analysis of Chevalier & Imamura (1982), but we take into account the transverse flow of material out of the postshock region. The mass loss from the postshock region stabilizes the flow. As a rough estimate, the shock radiative instability takes place when the shock wave position with no radiative cooling (only mass loss present) is larger than the shock position with no mass loss (only radiative cooling present).

For typical conditions of planetary nebulae we find that in order for the shock radiative overstability to occur, the nebular radius should be $R \gtrsim 10^{19} n_a^{-1}$ cm, where n_a is the total number density of the ISM (in units of cm^{-3}). We give several examples of interacting planetary nebulae in light of this condition.

1. INTRODUCTION

Langer Chanmugam & Shaviv (1981; 1982) pionered in calculating the radiative shock wave instability. They discussed the instability in the context of accretion column onto compact objects. Their initial work was extended to other astrophysical situations and for different physical parameters (Chevalier & Imamura 1982, hereafter CI; Imamura, Wolff & Durisen 1984; Langer 1985; Bertschinger 1986; Innes, Giddings & Falle 1987; Gaetz, Edgar & Chevalier 1988; Gouveia Dal Pino & Benz 1993). Bertschinger (1986) considered nonradial perturbations to a steady state one dimensional flow; and Gouveia Dal Pino & Benz (1993) found the radiative shock instability in their three dimensional hydrodynamical simulations. But most of the works mentioned above considered one dimensional flows. In this paper we consider another effect which results from multidimensional flow structure, namely, the transverse flow of material out of the postshock region.

For certain radiative cooling rates radiative shocks become overstable, i.e. the amplitude of a small perturbation of the shock position increases while it is oscillating around the shock equilibrium position. The cooling rate is mainly determined by the postshock temperature, which itself depends on the shock velocity. The cooling rate also depends on the preshock ionization levels of the different atoms. This can make a difference between ISM shock of planetary nebulae (PNe) and supernova remnants, since the central stars of PNe can ionize the preshock ISM.

Based on morphological considerations Zucker & Soker (1993) suggest that the interaction of the PN IC 4593 with the ISM possess the radiative shock instability. This PN clearly shows characteristics of PNe moving through the ISM, creating a bow shock in the ISM. The bow shock distance from the nebula is expected to be of the order of the nebula size (Soker, Borkowski & Sarazin 1991). The finite size of the bowshock, therefore, must be taken into account in calculating the shock instability.

In this paper we conduct semi-analytical study of the influence of a finite size shock region, by taking into account the mass which flows transversely out of the postshock region. Our technique and basic equations (§2.1), beside the mass loss term, are the same as those of CI. Our purpose is to examine the general influence of the transverse flow behind the bow shock on the radiative shock instability, rather than to study any particular object. We therefore describe the mass loss from the postshock region by a simple toy model (§2.2). In §3 we present the results. We look at the variation of the oscillation frequencies and growth rates of several modes and for several cooling rates, as the mass loss rate is varied. In §4 we discuss and summerize the implications of the results for PNe moving through the ISM.

2. THE EQUATIONS WITH SIDE MASS LOSS

2.1 The Basic Equations

Beside the mass loss term from the postshock region, our equations are the same as equation (1)-(3) of CI. The flow structure is illustrated in their figure 1, with the following notations. The spatial one dimensional coordinate is $x = x_s$ at the shock and $x = 0$ at the wall, where the postshock flow stagnates. ρ is the density, p is the pressure, v is the velocity along the x direction, and T is the temperature. The cooling rate per unit volume is $Ln_e n_p$, where n_e and n_p are the electron and proton density, respectively, and $L(T) \propto T^\alpha$ is the cooling function.

The flow equations for a $\gamma = 5/3$ gas, where γ is the adiabatic index, are (CI)

$$\frac{\partial \rho}{\partial t} + \rho \frac{\partial v}{\partial x} + v \frac{\partial \rho}{\partial x} = -\dot{\rho}_s \tag{2.1}$$

$$\rho \left(\frac{\partial v}{\partial t} + v \frac{\partial v}{\partial x} \right) + \frac{\partial p}{\partial x} = 0 \tag{2.2}$$

and

$$\frac{\partial p}{\partial t} + v \frac{\partial p}{\partial x} - \frac{5}{3} \frac{p}{\rho} \left(\frac{\partial \rho}{\partial t} + v \frac{\partial \rho}{\partial x} \right) = -\frac{2}{3} \rho^2 A \left(\frac{p}{\rho} \right)^\alpha , \tag{2.3}$$

where A is a constant. The only difference between (2.1)-(2.3) above and equations (1)-(3) of CI is the mass loss term $\dot{\rho}_s$ in equation (2.1). Therefore a steady state solution of our equations is not given in equations (7) and (8) of CI. The boundary conditions, though, are the same as those in CI. For an incoming preshock material with negligible temperature, density ρ_a and velocity $u_{\rm in}$ in the negative direction, the boundary conditions (i.e. the strong shock condition and the assumption of stationary wall) are (equations [4]-[6] of CI)

$$\rho_0(x_s) = 4\rho_a; \qquad v_0(x_s) = -\frac{1}{4}u_{\rm in}; \qquad p_0(x_s) = \frac{3}{4}\rho_a u_{\rm in}^2; \qquad v_0(0) = 0. \tag{2.4}$$

We note that around finite size objects there will be bow shocks. The shock conditions away from the symmetry axis should be those for oblique shocks. In our one-dimensional analysis we neglect this effect. In any case, this effect is small in our problem since we look on the flow near the symmetry axis. The finite size of the object is taken into account by the introduction of the mass loss term.

We follow CI and allow the shock wave to be perturbed by

$$\frac{dx_s}{dt} = v_{s1}e^{\omega t}, \tag{2.5}$$

so that the shock position is at

$$x_s = x_{s0} + x_{s1}e^{\omega t}, \tag{2.6}$$

where $x_{s1} = v_{s1}/\omega$, and a null subscript describes a steady state value while a subscript 1 describes a first-order term. $w = \omega_R + i\omega_I$ is a complex number, whereas v_{s1} is real. We define the dimensionless variable (CI eq. [16])

$$\xi = \frac{x}{x_s} = \frac{x}{x_{s0}}\left(1 - \frac{x_{s1}}{x_{s0}}e^{\omega t}\right), \tag{2.7}$$

where in the second equality we kept only first order terms. To the same order, CI find

$$\frac{\partial\xi}{\partial x} = \frac{1}{x_{s0}}\left(1 - \frac{x_{s1}}{x_{s0}}e^{\omega t}\right); \qquad \frac{\partial\xi}{\partial t} = -\frac{x x_{s1}\omega e^{\omega t}}{x_{s0}^2}. \tag{2.8}$$

The perturbed physical variables take the form

$$\rho(\xi,t) = \rho_0(\xi) + \rho_1(\xi)e^{\omega t}, \tag{2.9}$$

and similar expressions for the pressure and velocity. The boundary conditions at the shock wave (2.4) become (CI eqs. [21]-[23])

$$\rho_1 = 0; \qquad v_1 = \frac{3}{4}v_{s1}; \qquad p_1 = \frac{3}{2}\rho_a\, u_{\rm in} v_{s1}. \tag{2.10}$$

To obtain the first-order equations we substitute the physical variables from expressions (2.9) into the fluid equations (2.1)-(2.3). Following CI we simplify the first order equations by the following variables transformation

$$\zeta = \frac{x_{s0}\omega}{v_{s1}}\frac{\rho_1}{\rho_a}; \qquad \pi = \frac{p_1}{\rho_a\, u_{\rm in} v_{s1}}; \qquad \eta = \frac{v_1}{v_{s1}}; \tag{2.11}$$

using $w = v_0/u_{\rm in}$ as the independent variable, and by introducing $\delta = x_{s0}\omega/u_{\rm in}$. The steady state flow with a mass loss term cannot be expressed in a compact form (unlike equations [7] and [8] of CI) and our first-order equations are somewhat more complicated (compare with [27]-[29] of CI). We take the mass loss term $\dot{\rho}_s$ in equation (2.1) from equation (2.16) which we derive in the next section. Our first- order equations read

$$\frac{d\eta}{dw}\hat{\rho}_0 + \frac{d\zeta}{dw}\frac{w}{\delta} = -\frac{d\hat{\rho}_0}{dw}\eta + \frac{d\hat{\rho}_0}{dw}\xi - \frac{d\xi}{dw}\zeta - \frac{\zeta}{\delta} - \frac{d\xi}{dw}\frac{\epsilon x_{s0}}{R}\left(\frac{5}{3}\right)^{1/2}\left(\frac{\zeta}{\delta}\sqrt{\frac{\hat{p}_0}{\hat{\rho}_0}} + \pi\sqrt{\frac{\hat{\rho}_0}{\hat{p}_0}} + \frac{2\sqrt{\hat{p}_0\,\hat{\rho}_0}}{\delta}\right) \tag{2.12}$$

$$\frac{d\pi}{dw}\frac{1}{\hat{\rho}_0} + \frac{d\eta}{dw}w = -\eta - \frac{d\xi}{dw}\delta\,\eta + \xi - \frac{w\,\zeta}{\delta\,\hat{\rho}_0} \tag{2.13}$$

and

$$\begin{aligned}\frac{d\pi}{dw}w - \frac{5\,\hat{p}_0\,w}{3\,\delta\,\hat{\rho}_0}\frac{d\zeta}{dw} &= -\frac{d\xi}{dw}\delta\,\pi + \frac{5\,\pi\,w}{3\,\hat{\rho}_0}\frac{d\hat{\rho}_0}{dw} + \eta\,\hat{\rho}_0\,w - \frac{\hat{\rho}_0\,w^2}{\delta} - \hat{\rho}_0\,w\,\xi \\ &- \left(\frac{5\,\hat{p}_0\,w}{3\,\hat{\rho}_0}\frac{d\hat{\rho}_0}{dw} + \hat{\rho}_0\,w^2\right)\left(\frac{\alpha\,\pi}{\hat{p}_0} + (2-\alpha)\frac{\zeta}{\delta\,\hat{\rho}_0}\right) \\ &+ \frac{5\,\hat{p}_0}{3\,\hat{\rho}_0}\left(\frac{d\hat{\rho}_0}{dw}\eta - \frac{d\hat{\rho}_0}{dw}\xi + \frac{d\xi}{dw}\zeta - \frac{d\hat{\rho}_0}{dw}\frac{w}{\delta} - \frac{d\hat{\rho}_0}{dw}\frac{w\zeta}{\delta\,\hat{\rho}_0}\right)\end{aligned} \tag{2.14}$$

where $\hat{\rho}_0 = \rho_0/\rho_a$ and $\hat{p}_0 = p_0/(\rho_a u_{in}^2)$.

When these three equations are separated into their real and imaginary parts we have six equations. These are suplemented with the boundary conditions at the shock wave $w = -1/4$, given by equation (2.10): $\zeta_R = \zeta_I = 0$, $\pi_R = 3/2$, $\pi_I = 0$, $\eta_R = 3/4$, and $\eta_I = 0$, and the boundary conditions $\eta_R = \eta_I = 0$ at the stationary wall $w = 0$. The eight boundary conditions for the six quations determine the eigenvalues δ_R and δ_I. Positive value of δ_R means an unstable solution. Subscripts R and I stand for real and imaginary parts, respectively. There are two parameters in the problem, the power of the temperature in the cooling function α, and the mass loss rate, which we parametrize by β, which is defined in the next subsection.

2.2 The Mass Loss Term

We take the post shock region to be a cylinder, with its axis along the x axis, and its radius R equals to the radius of the solid body that supports the shock wave. We assume that the physical variables describing the post-shock gas are function of x only, which is compatible with the one dimensional flow equations (2.1)-(2.3). We assume that the gas at the cylinder envelope streams transversely out of the postshock region at a fraction ϵ of the adiabatic sound speed $v_s(x) = \sqrt{\gamma P(x)/\rho(x)}$. The mass loss rate from a slice of width Δx is given by

$$\dot{M}(x) = 2\pi R \Delta x \rho(x) \epsilon v_s(x). \tag{2.15}$$

Since the volume of the slice is $V = \pi R^2 \Delta x$, the density variation due to this mass loss is

$$\dot{\rho}(x) = \frac{\dot{M}(x)}{V} = 2\epsilon \frac{\rho(x) v_s(x)}{R}. \tag{2.16}$$

This expression was used in deriving equation (2.12) from equation (2.1). This expression of sideway mass loss introduces a new scale length to the problem R/ϵ. The cooling term, the r.h.s. of equation (2.3), introduces the scale length $l = u_{\rm in}^{3-2\alpha}/(\rho_a A)$. We define the parameter $\beta \equiv \epsilon l/R$, which will appear in the equations below.

To better understand the nature of the mass loss term, let us write the steady state solution with mass loss but without cooling, $A = 0$ in equation (2.3). The energy equation (2.3) becomes

$$P_0 = K\rho_0^{5/3}, \tag{2.17}$$

where K is a constant in the postshock region. The steady state version of the mass conservation equation (2.1) is

$$\frac{d}{dx}(\rho_0 v_0) = -\dot{\rho}_0 = -\frac{2\epsilon}{R}\left(\frac{5}{3}\right)^{1/2} P_0^{1/2}\rho_0^{1/2} = -\frac{2\epsilon}{R}\left(\frac{5}{3}\right)^{1/2} K^{1/2}\rho_0^{4/3} \tag{2.18}$$

where in the second equality we have substitute for $\dot{\rho}$ from equation (2.16), and in the third we used the energy equation (2.17). We substitute P_0 from equation (2.17) in the steady state version of the momentum equation (2.2), which after some rearrangements reads

$$\frac{1}{2}\frac{dv_0^2}{dx} = -\frac{5K}{2}\frac{d\rho_0^{2/3}}{dx}. \tag{2.19}$$

Integration of the last equation, with the boundary conditions $v(x_{m0}) = -u_{\rm in}/4$ and $\rho(x_{m0}) = 4\rho_a$, gives

$$\rho_0 = (5k)^{-3/2}(u_{\rm in}^2 - v_0^2)^{3/2}, \tag{2.20}$$

where x_{m0} is the steady state shock position when there is no cooling. Substituting ρ_0 from the last equation in the mass conservation equation (2.18) gives, after some manipulation,

$$(u_{\rm in}^2 - 4v_0^2)(u_{\rm in}^2 - v_0^2)^{1/2}\frac{dv_0}{dx} = -\frac{2\epsilon}{3^{1/2}R}(u_{\rm in}^2 - v_0^2)^2. \tag{2.21}$$

We now define $w \equiv v_0/u_{\rm in}$, and integrate equation (2.21) from $w(0) = 0$ to w, and from $x = 0$ to x. The solution for x is

$$x = \frac{3^{1/2}R}{2\epsilon}\left[\frac{3w}{(1-w^2)^{1/2}} - 4\arcsin w\right]. \tag{2.22}$$

To obtain the solution for the steady state shock position x_{m0} we substitute $w(x_{m0}) = -1/4$

$$x_{m0} = \frac{3^{1/2}R}{2\epsilon}\left[-\frac{3}{(15)^{1/2}} + 4\arcsin(1/4)\right] = 0.204R/\epsilon. \tag{2.23}$$

To better illustrate the steady state solution we plot in figures 1-3 the density, the isothermal sound speed squared, and the velocity of the flow, respectively, versus $\xi = x/x_s$, for $\alpha = -1/2$ and three values of β.

To estimate the value of $\beta = \epsilon u_{\rm in}^{3-2\alpha}/(\rho_a AR)$ above which mass loss is significant, we evaluate the steady state energy equation (2.3) for the case without mass loss. We note, as CI point out, that for specific values of α there are analytical solutions. We would like, though, to obtain an approximate expression for any value of α. We assume a constant presure which equals $\rho_a u_{\rm in}^2$ and use equations (7) and (8) of CI. This assumption is equivalent to taking only the lowest order terms in v_0 of equation (9) of CI. The steady state energy equation reads now

$$5(-v_0)^{2-\alpha} u_{\rm in}^{1-\alpha} dv_0 = -2\rho_a u_{\rm in} A dx. \tag{2.24}$$

Integrating from $v_0 = 0$ to $v_0 = -1/4$ and from $x = 0$ to $x = x_{c0}$, and using the definition of β gives

$$\frac{5}{2}\frac{4^{\alpha-3}}{3-\alpha} = \beta^{-1}\frac{x_{c0}\epsilon}{R}, \tag{2.25}$$

where x_{c0} is the shock position without the mass loss process. Substituting $x_{c0} = x_{m0}$ and $x_{m0} = 0.2R/\epsilon$ from equation (2.23), gives the value of β above which mass loss significantly alters the eigenvalue δ.

$$\beta_c = 0.08(3-\alpha)4^{3-\alpha}. \tag{2.26}$$

For $\alpha = -2$, -0.5, 0, and 0.5, for example, we find $\beta_c = 410$, 36, 15, and 6.4, respectively.

3. SOLUTION OF THE EQUATIONS

As discussed in the end of section 2.1, seperating equations (2.12)-(2.14) to real and imaginary parts results in 6 equations with 8 boundary conditions. These 6 equations are coupled to the steady state equations (2.1)-(2.3) with the 4 boundary conditions (2.4).

There are in total 9 equations for the 9 variables ρ_0, p_0, v_0, ζ_R,ζ_I,π_R,π_I,η_R and η_I. The 12 boundary conditions determine the 3 additional unknowns x_{s0} and the eigen frequencies δ_R and δ_I.

This is a 2 point boundary value problem that we solved with the shooting method. Starting with no mass loss $\beta = 0$, we recovered the solution of CI. We then increased the the mass loss by increasing β. The results are depicted in figures $4 - 10$. The figures show the real (δ_r) and imaginary (δ_i) eigenvalues (frequencies) as a function of β for different cooling laws α and different oscillatory modes.

From the graphs we see that the mass loss term has a stabilizing effect for all cases. As indicated by equation (2.26) the stabilizing effect is weaker for low values of α (Figs. 4 and 5). The values of β at which the fundamental modes become stable are $\beta = 950, \quad 100, \quad 28, \quad 5$, and 3, for $\alpha = -2, \quad -1, \quad -0.5, \quad 0$, and 0.5, respectively. These results are in good agreement with the analytical formula (2.26).

For all the fundamental modes the real part of δ decreases more rapidly than the imaginary part. Since the imaginary part is not influenced a lot by the mass loss rate, the growth rate per oscillation is damped at the same rate as δ_R decreases. For the overtones (figs. 8 and 9) the imaginary part decreases more rapidly than δ_R which means that per oscillation period, the rate of damping by the mass loss of the instability is lower than the absolute decrease in δ_r.

4. DISCUSSION

We now apply our results to the interaction of PNe with the ISM. Since the central stars of PNe are likely to ionize the preshock ISM under some circumstances, we assume a fully ionized preshock gas. We write the constant A which appear in equation (2.3) in

term of the cooling function $L(\,\mathrm{ergs\,cm^3\,s^{-1}})$ used by of Gaetz *et al.* (1988)

$$A = L\frac{n_e n_p}{\rho^2}\left(\frac{P}{\rho}\right)^{-\alpha}, \tag{4.1}$$

where n_e and n_p are the electron and proton density, respectively. Using the expressions for the pressure and density behind a strong shock for a gas of adiabatic index γ, we find

$$\frac{P_s}{\rho_s} = \frac{2(\gamma-1)}{(\gamma+1)^2}\,u_{\rm in}^2. \tag{4.2}$$

Substituting equation (4.2) into (4.1) and taking fully ionized solar abundance gas with $\gamma = 5/3$ yields the expression for A in c.g.s. units

$$A = 2\times 10^{25}(16/3)^{\alpha}\,u_{\rm in}^{-2\alpha}\left(\frac{L}{10^{-22}\,\mathrm{ergs\,cm^3\,s^{-1}}}\right). \tag{4.3}$$

We now substitute this expression of A in the definition of $\beta = \epsilon\, u_{\rm in}^{3-2\alpha}/(\rho_a A R)$. Scaling with physical parameters typical of PNe we find

$$\beta = 163(3/16)^{\alpha}\epsilon n_a^{-1}\left(\frac{L}{10^{-22}\,\mathrm{ergs\,cm^3\,s^{-1}}}\right)^{-1}\left(\frac{R}{10^{18}\,\mathrm{cm}}\right)^{-1}\left(\frac{u_{\rm in}}{150\,\mathrm{km\,s^{-1}}}\right)^{3}, \tag{4.4}$$

where n_a is the total ISM number density in $\mathrm{cm^{-3}}$ and R the nebular radius. For typical parameters of PNe, we find from Geatz *et al.* (1988) that $-0.5 \lesssim \alpha \lesssim 0$. From figures 6 and 7 we find that the criteria for instability for $\alpha = -0.5$ and $\alpha = 0$ are $\beta < 28$ and $\beta < 5$, respectively. From figures 2 and 3 of Gaetz *et al.* (1988) we see that $\alpha = -0.5$ for $u_{\rm in} \simeq 200\,\mathrm{km\,s^{-1}}$, and $\alpha \simeq 0$ for $u_{\rm in} \simeq 150\,\mathrm{km\,s^{-1}}$. Using these with the typical physical parameters of equation (4.4), the criterion for radiative shock instability to occur is

$$\frac{R}{10^{18}\,\mathrm{cm}} \gtrsim \frac{32\epsilon}{n_a}, \tag{4.5}$$

where the ISM density n_a is in $\mathrm{cm^{-3}}$. From figure 2 of Soker *et al.* 1991 we see that matter leaves the postshock region at $\sim 30\%$ of the sound speed, so that $\epsilon \sim 0.3$. Using this in equation (4.5), we obtain the condition for radiative shock overstability

$$R \gtrsim 10^{19}\left(\frac{n_a}{\mathrm{cm^{-3}}}\right)^{-1}\,\mathrm{cm}. \tag{4.6}$$

We remind that R is the PN radius and n_a the total number density of the undisturbed ISM. In general, equation (4.6) implies that only large PNe, with radius of $\gtrsim 1\,\mathrm{pc}$, which resides near the galactic plane , where the density of the warm medium is $n_a \sim 1\,\mathrm{cm}^{-3}$, will possess the radiative shock overstability. We point out that equation (4.6) was derived by using a toy model, and can be off by up to an order of magnitude. A two-dimensional numerical simulation is needed to obtain a more accurate expression.

Let us examine few nebulae in light of the results expressed by equation (4.6). One of the best example of interacting PN is A35 (Jacoby 1981). The radius of A35 is 0.8 pc (Jacoby 1981), the relative velocity is $\sim 125\,\mathrm{km\,s}^{-1}$, and the ISM density is $\sim 0.1\,\mathrm{cm}^{-3}$ (Borkowski, Sarazin & Soker 1990). Using these values in equation (4.6), we do not expect the interaction of A35 with the ISM to possess the radiative shock overstability.

Next we examine IC 4593, which Zucker & Soker (1993) suggest possesses the radiative shock overstability. However, this PN resides 1.6 kpc above the galactic plane, where the density is very low, and has a radius of $0.25\,\mathrm{pc} = 7.5\times10^{17}$ cm, which according to equation (4.6) mean that IC 4593 should not possess the instability. There are three ways out of the discrepancy with Zucker & Soker conjecture. First, it is possible that the suggestion of Zucker & Soker, which is based on morphological features, is wrong. Second, it is possible that the main nebula of IC 4593 is running into a much denser medium, which was formed by IC 4593 itself in an earlier mass loss episode. Third, at late stage of the interaction the front edge of the nebula become distorted. This can cause the stream along, and near, the line that goes through the center of the nebula to continue flowing in the preshock direction, instead of leaving the postshock region. This can be seen in figure 2 of Soker *et al.* (1991). To test the last two processes a two-dimensional time dependent numerical code which includes radiative cooling is required.

Table 1 of Borkowski *et al.* (1990) contains nine PNe with large proper motion.

Of these, NGC 7293 (the Helix nebula), S216, and NGC 6853 are large enough and close enough to the galactic plane to have the conditions for the radiative shock overstability. However, these three PNe do not have high enough velocities. It is possible, though, that their total velocity, including the line of sight velocity, relative to the ISM is above $140\,\mathrm{km\,s^{-1}}$, which is the condition for overstability (Gaetz *et al.* 1988). Table 2 of Borkowski *et al.* contains a list of large PNe, for most whom proper motion do not exist. It is likely that some of them obey the overstability condition (4.6) and have large enough relative velocity. Future study of these PNe should look for the radiative shock overstability.

Tweedy & Kwitter (1994) study four PNe which interact with the ISM. These PNe, A 31, A 34, A61 and A 62, are large and close to the galactic plane (Kaler 1983). Another intersting PN is Sh 2-174,which is at a very advance stage of interaction with the ISM (Tweedy & Napiwotzki 1994). The radii of these PNe fall short by factors of several from obeying condition (4.6) for overstability (unless they are situated in high density environments). Remembering that condition (4.6) can be of by up to an order of magnitude, and due due to some uncertainties as with IC 4593 which we mentioned above, it is possible that these PNe posses the radiative shock overstability. Future studies should determine the relative velocity with respect to the ISM, and carefully look for signs of radiative shock overstability.

The radiative overstability could also be important at the working surfaces of stellar jets (Herbig-Haro objects), as the recent hydrodynamical simulations (Gouveia Dal Pino & Benz 1993) indicate. In this case the ambient density ranges from 100 to 1000 $\mathrm{cm^{-3}}$ (Morse et al 1993), the jet cross sections are $\sim 10^{16}$ cm and the velocities are $\sim 150\,\mathrm{km\,s^{-1}}$. By expression (4.6) we see that the radiative shock overstability is likely to occur in these systems.

The research described in this paper was carried out by the Jet Propulsion Laboratory, California Institute of Technology, under a contract with the National Aeronautics and Space Administration. We would like to thank Amiel Sternberg for the hospitality at Tel-Aviv University and Alberto Noriega-Crespo for a careful reading of the manuscript and useful suggestions.

R.D. has been supported by the Swiss National Foundation.

N.S. has been supported by the Allon Fellowship in Israel.

REFERENCES

Bertschinger, E. 1986, ApJ, 304, 154.

Borkowski, K. J., & Sarazin, C. L., & Soker, N. 1990, ApJ, 360, 173.

Chevalier, R. A., & Imamura, J. N. 1982, ApJ, 261, 543 (CI).

Gaetz, T. J., Edgar, R. J., & Chevalier, R. A. 1988, ApJ, 329, 927.

Gouveia Dal Pino, E. M., & Benz, W. 1993, ApJ, 410, 686.

Imamura, J. N., Wolff, M. T., & Durisen, R. H. 1984, ApJ, 276, 667.

Innes, D. E., Giddings, J. R., & Falle, S. A. E. G. 1987, MNRAS, 226, 67.

Jacoby, G. H. 1981, ApJ, 244, 903.

Kaler J. B. 1983, ApJ, 271, 188.

Langer, S. H. 1985, in *Cataclysmic Variables and Low-Mass X-ray Binaries*, ed. D. Q. Lamb and J. Patterson (Dordrecht: Reidel), p. 257.

Langer, S. H., Chanmugam, G., & Shaviv G. 1981, ApJ Lett., 245, L23.

Langer, S. H., Chanmugam, G., & Shaviv G. 1982, ApJ, 258, 289.

Morse, J. A., Hartigan, P., Cecil, G., Heathcole, S. R., & Raymond, J. C. 1993, ApJ, 410, 764.

Soker, N., Borkowski, K. J., & Sarazin, C. L. 1991, AJ, 102, 1381.

Tweedy, R. W., & Kwitter, K. B. 1994, preprint.

Tweedy, R. W., & Napiwotzki, R. 1994, preprint.

Zucker, D. B. & Soker, N. 1993, ApJ, 408, 579.

FIGURE CAPTIONS

Fig. 1: The steady state logarithm of the normalized density for the cooling exponent $\alpha = -1/2$, for different mass loss rates as expressed by the parameter β. The absissa is $\log(\xi) = \log(x/x_s)$. The solid line represents $\beta = 0$, the dotted line $\beta = 40$ and the dashed line $\beta = 80$. The value of β needed to stabilize the fundamental mode in this case is $\beta = 28$.

Fig. 2: The steady state normalized isothermal sound speed squared $P_0/\rho_0/u_{in}^2$ for the cooling exponent $\alpha = -1/2$, for different mass loss rates as expressed by the parameter β as in Fig.1. The absissa is $\xi = x/x_s$.

Fig. 3: The steady state normalized velocity $w = u/u_{in}$ for the cooling exponent $\alpha = -1/2$, for different mass loss rates as expressed by the parameter β as in Fig.1. The absissa is $\xi = x/x_s$.

Fig. 4: The real (δ_R) and imaginary (δ_I) eigenvalues for the cooling exponent $\alpha = -2$ fundamental mode, as a function of the mass loss rate as expressed by β.

Fig. 5: The same for the case $\alpha = -1$ fundamental mode.

Fig. 6: The same for the case $\alpha = -1/2$ fundamental mode.

Fig. 7: The same for the case $\alpha = 0$ fundamental mode.

Fig. 8: The same for the case $\alpha = 0$ first overtone.

Fig. 9: The same for the case $\alpha = 0$ second overtone.

Fig. 10: The same for the case $\alpha = 1/2$ fundamental mode.

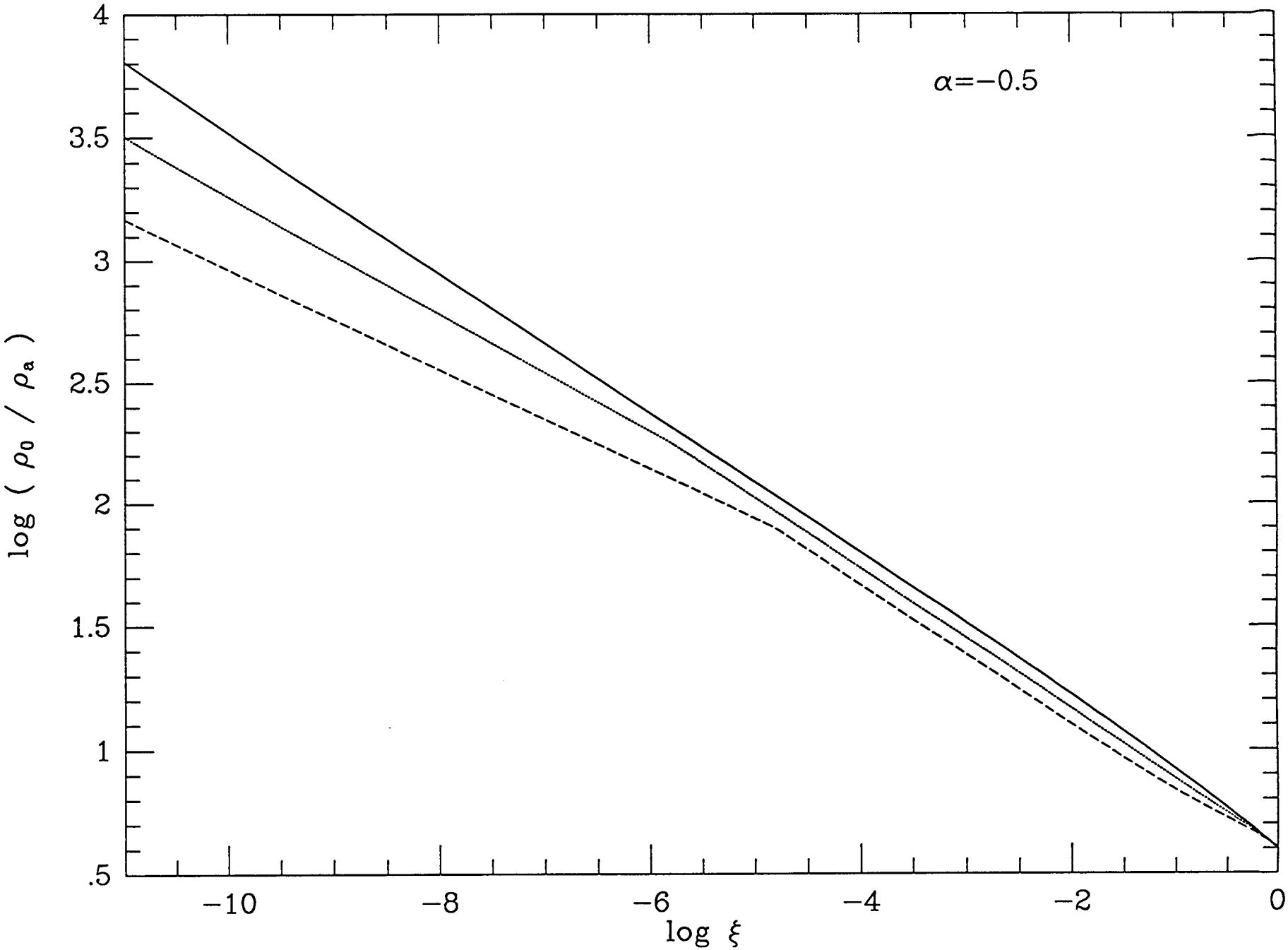

Fig. 1

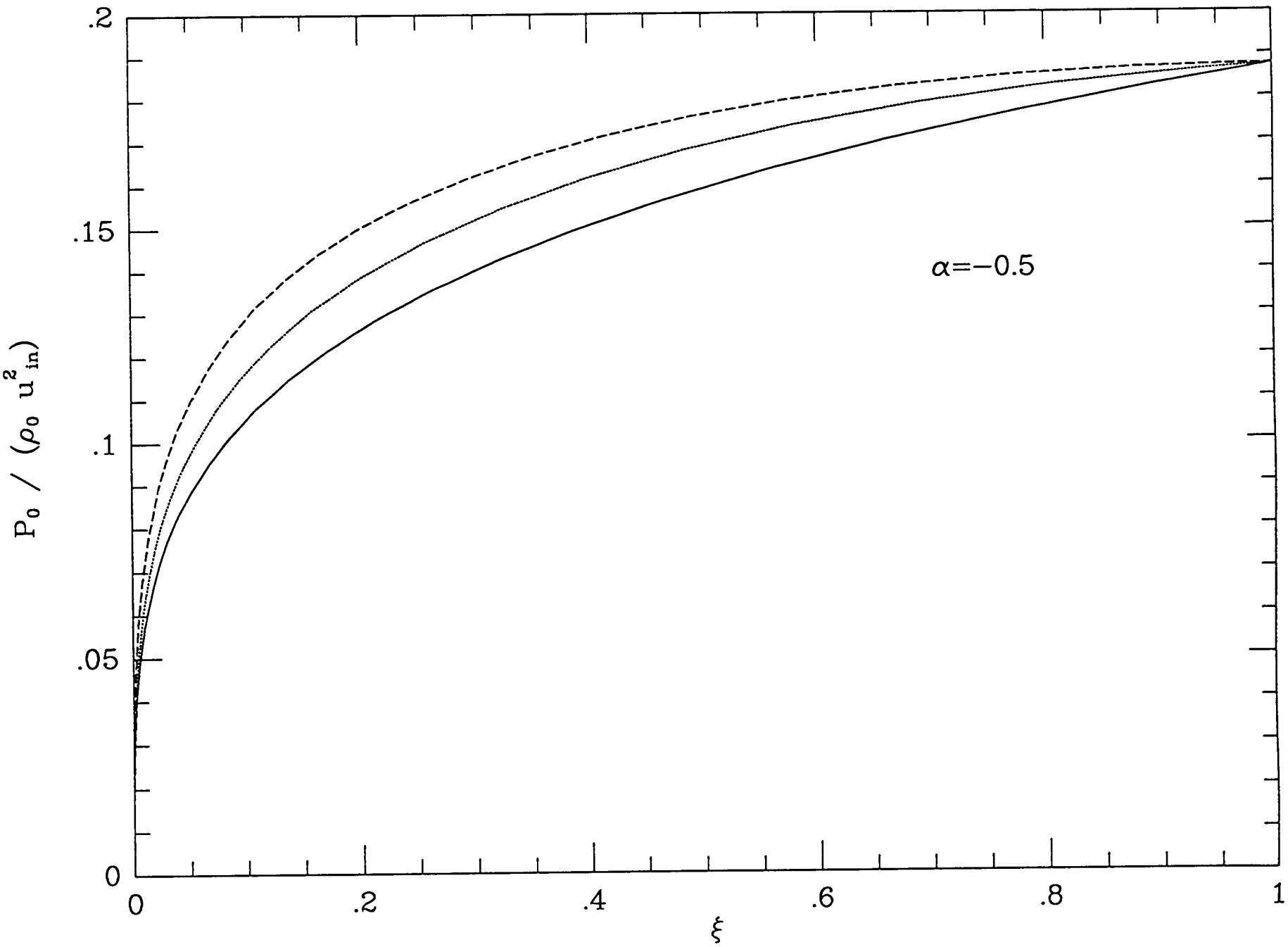

Fig. 2

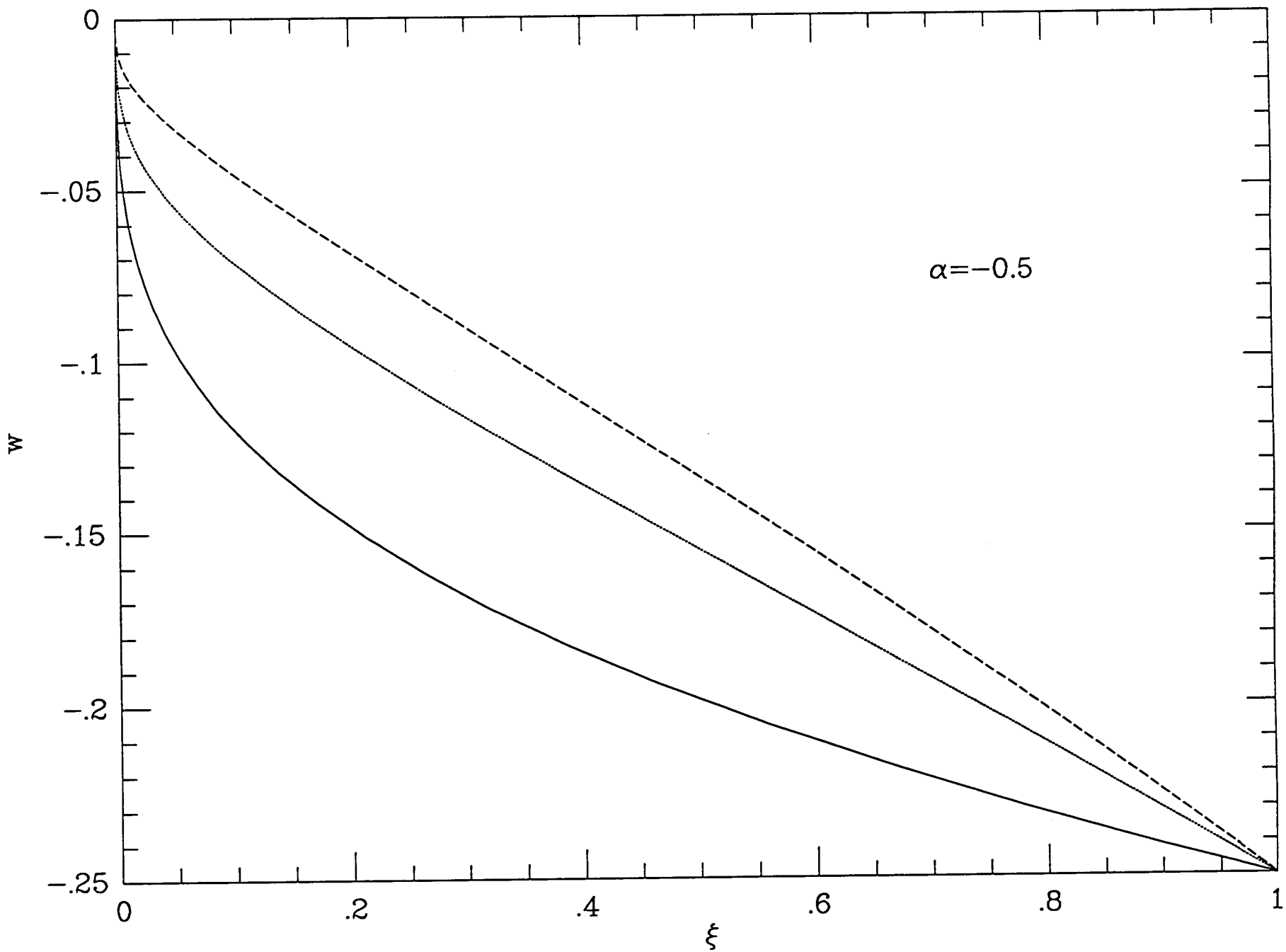

Fig. 3.

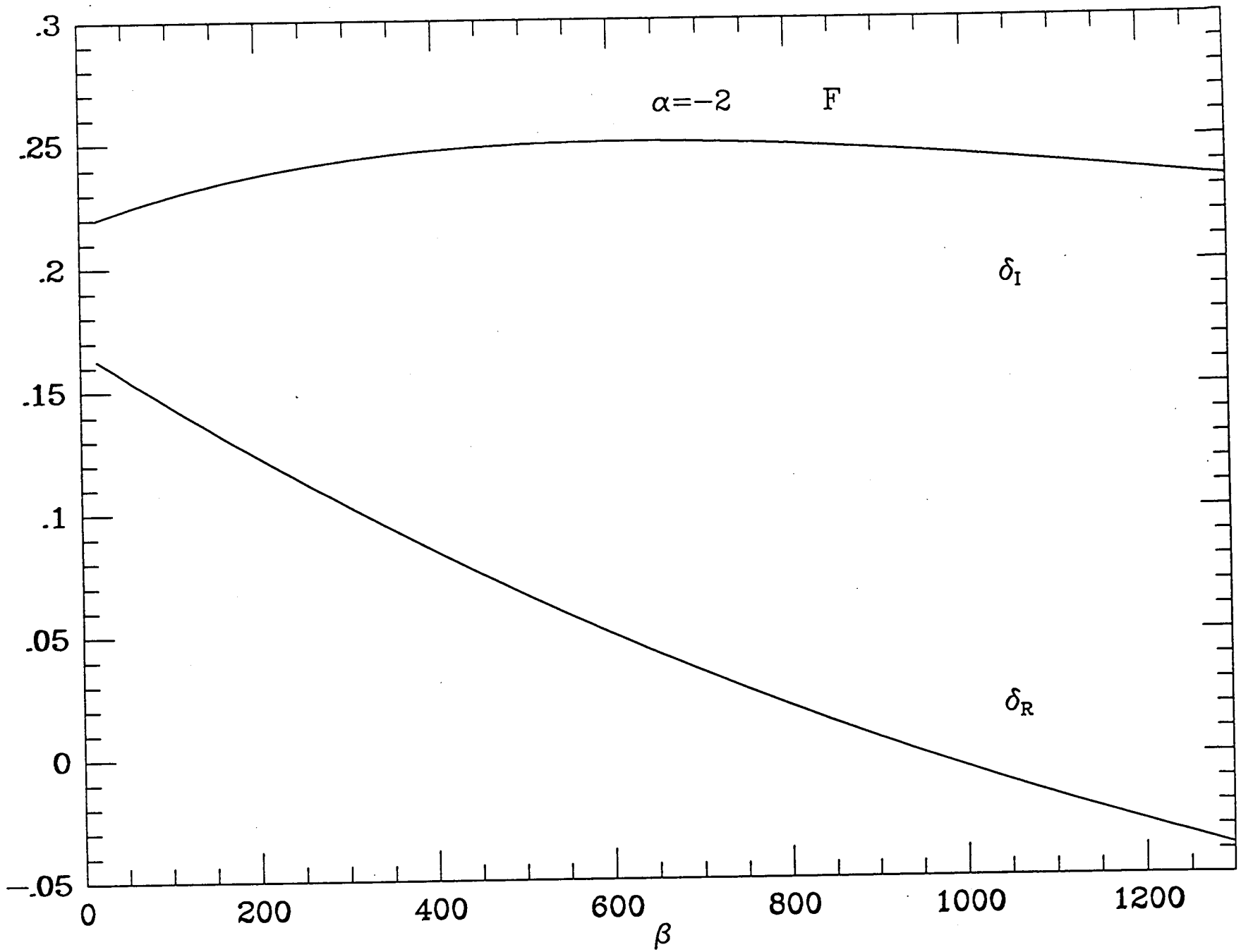

Fig. 4

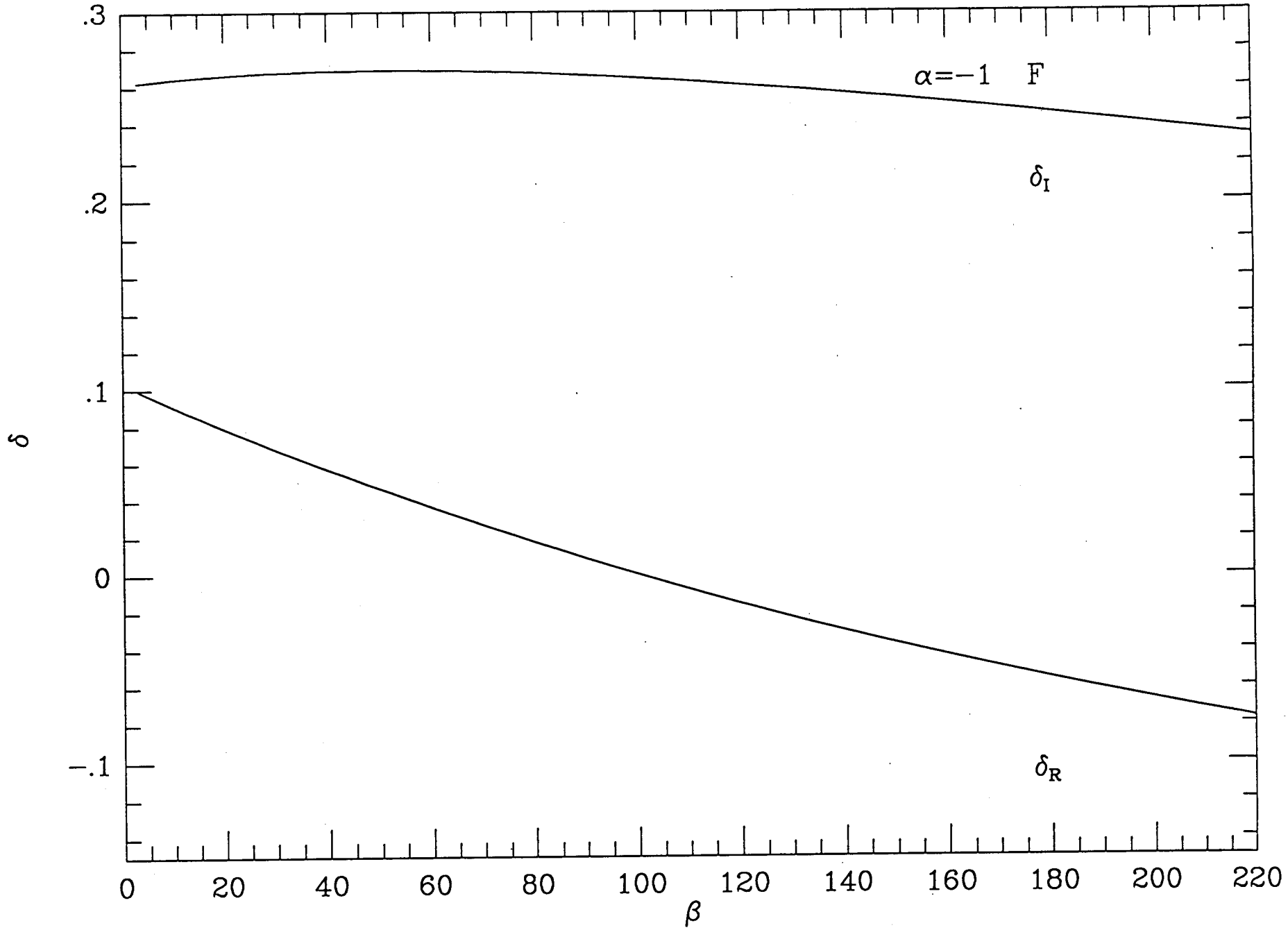
.3
.2
.1
0
−.1
δ
α=−1 F
δ_I
δ_R
0
20
40
60
80
100
120
140
160
180
200
220
β

Fig. 5

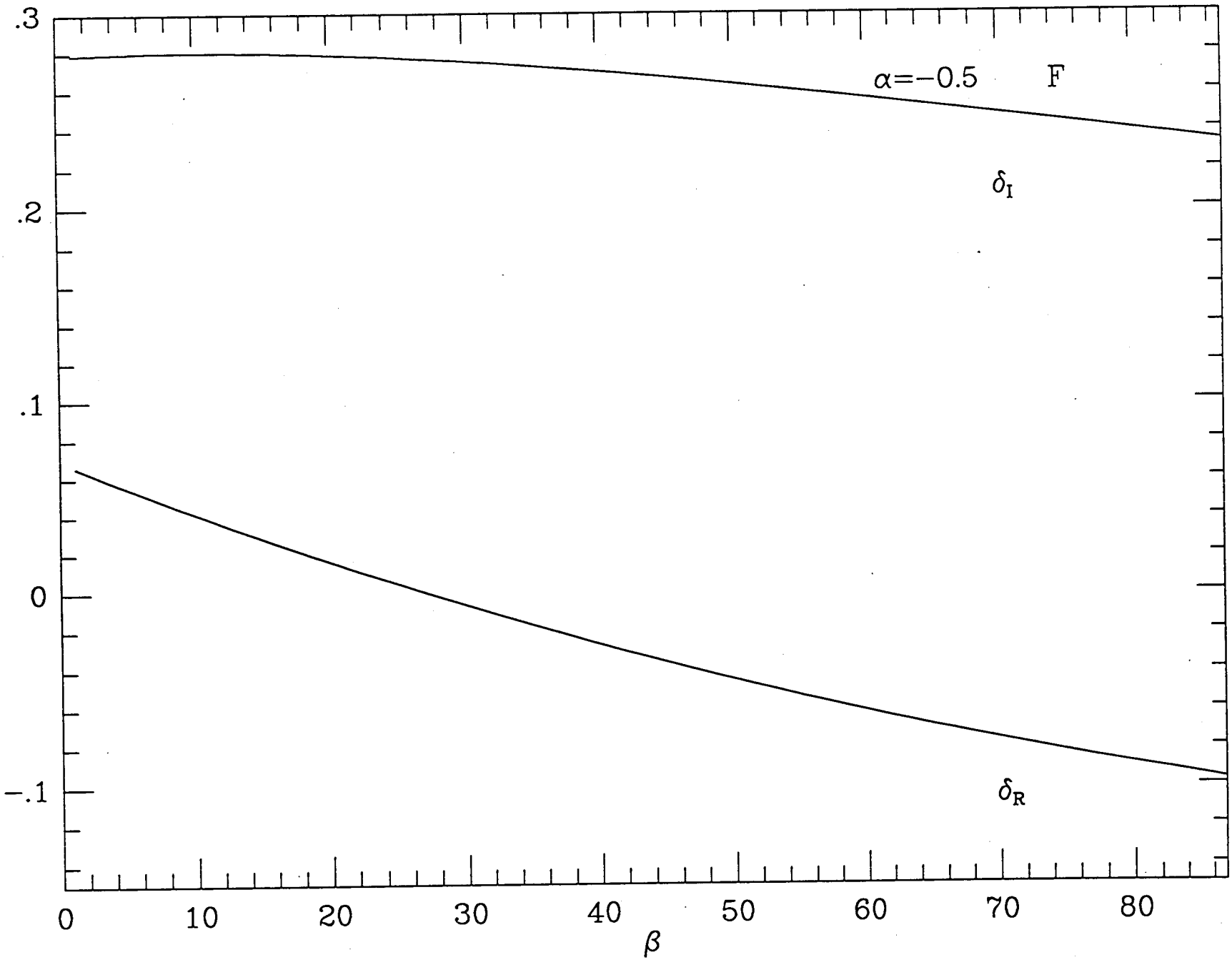

Fig. 6

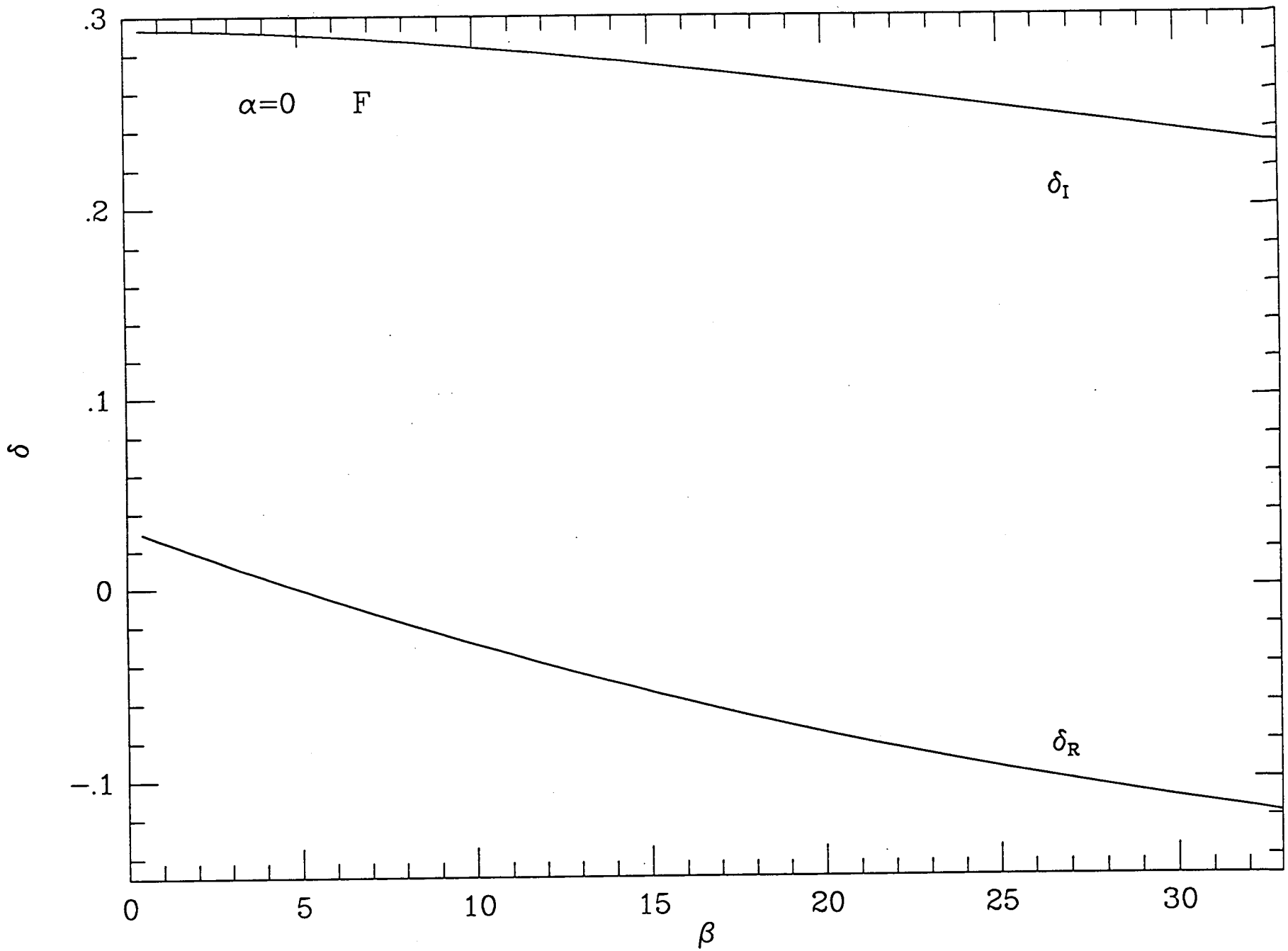

Fig. 7

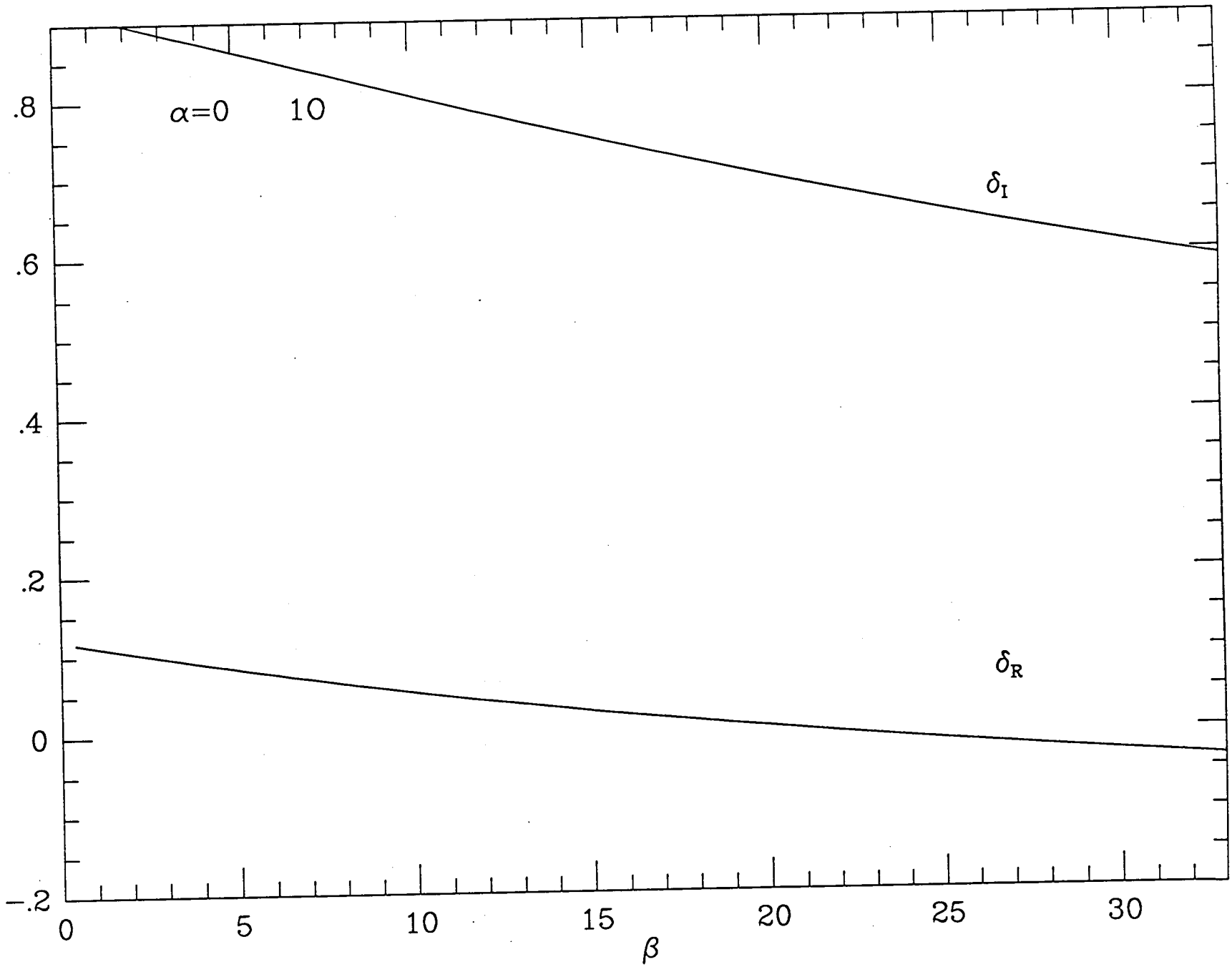

Fig. 8

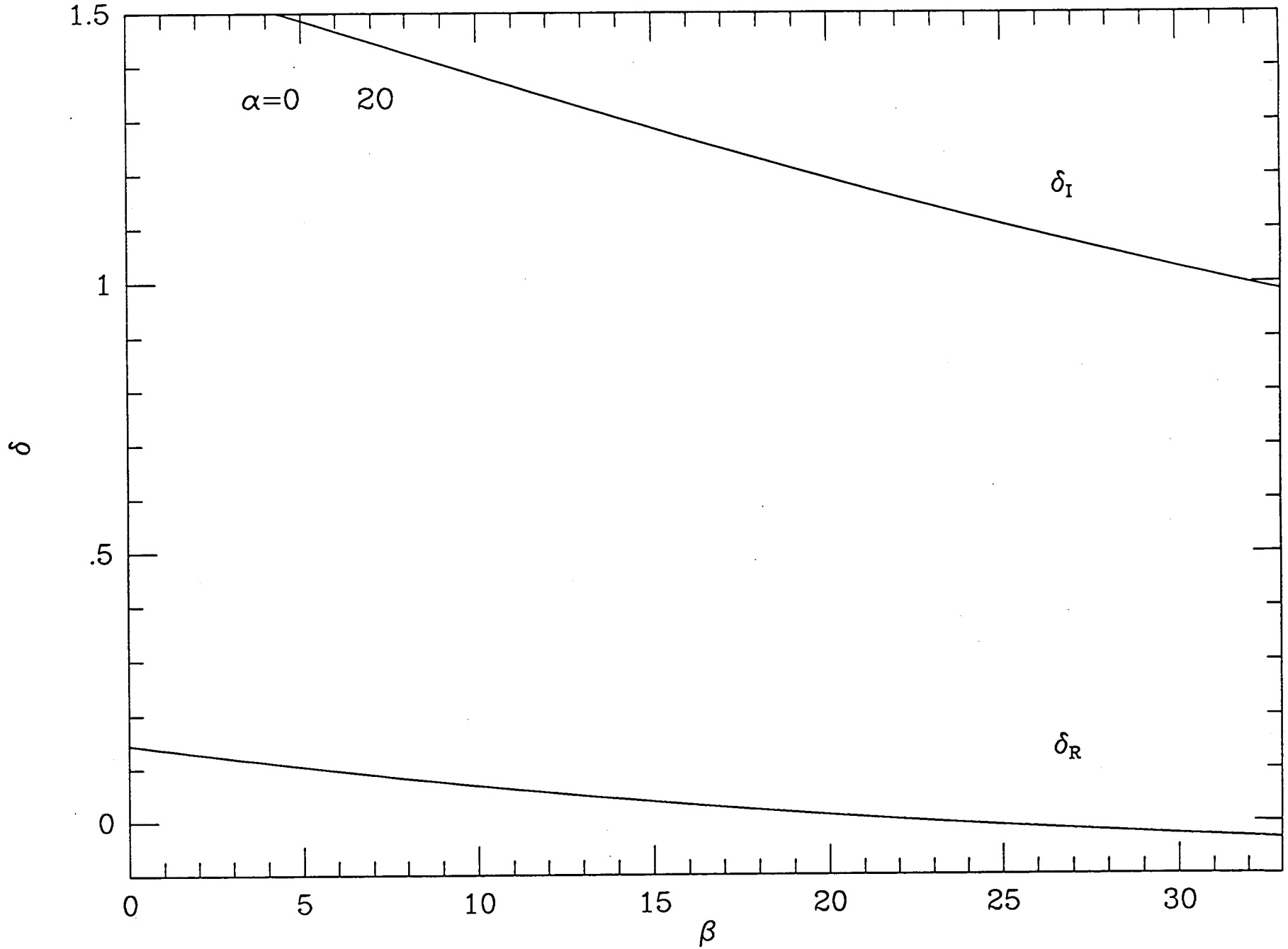

Fig. 9

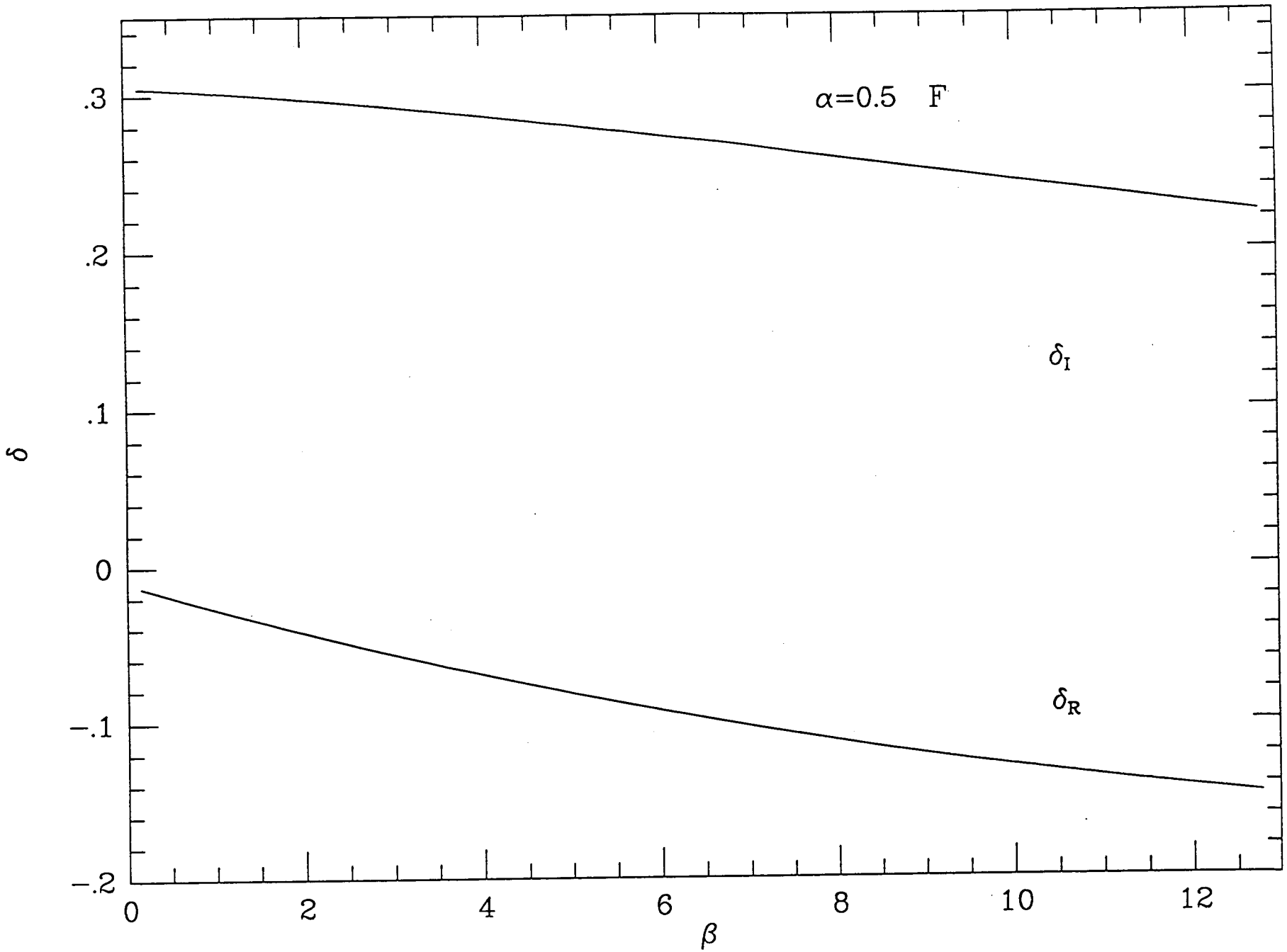

Fig. 10